Supporting information for

Interfacial Electron Modulation for Ru Particles on Cu Aerogel as Efficient Electrocatalyst for Hydrogen Evolution Reaction

Haoxin Fan[a,b,#], Xinhao Wan[a,#], Yarui Tang[a], Jianqi Ye[a,b], Jie Gao[c], Wei Gao[a,b,*], Dan Wen [a,*]

[a] *State Key Laboratory of Solidification Processing, School of Materials Science and Engineering, Northwestern Polytechnical University, Xi'an, 710072, P. R. China*

[b] *Research & Development Institute of Northwestern Polytechnical University in Shenzhen, Shenzhen, 518057, P. R. China*

[c] *School of Life Sciences, Northwestern Polytechnical University, Xi'an, 710072, P. R. China*

* Corresponding authors.

[#] H. Fan and X. Wan contributed equally to this work.

* Corresponding authors should be addressed to W. Gao (wei.gao@nwpu.edu.cn) and D. Wen (dan.wen@nwpu.edu.cn).

Experimental

1. Materials and Chemicals

Copper (II) chloride tetrahydrate ($CuCl_2 \cdot 2H_2O$, 99.999 %) was obtained from Aladdin Industrial Corp (China). Ruthenium (III) chloride hydrate ($RuCl_3 \cdot xH_2O$, 99.99 %) was purchased from Shanghai Yuanye Bio-Technology Co. Ltd. Sodium borohydride ($NaBH_4$) was purchased from Sigma-Aldrich Co. Ltd. Nafion solution (5 wt%) was bought from Alfa Aesar. Ethanol (C_2H_6O, AR), acetone (C_3H_6O, AR) and concentrated sulfuric acid (H_2SO_4, 98%) were provided from Sinopharm Chemical Regent Co. Ltd (China). Pt/C JM (20 wt%) was obtained from Shanghai hesen electric Co. Ltd. Carbon fiber paper (TGP-H-060) was acquired from Toray Co. Ltd. All the chemicals were used without further purification, and all the solutions were prepared using Milli-Q deionized water with the resistivity of 18.2 $M\Omega \cdot cm$.

2. Synthesis of Ru-Cu and Cu aerogels

Ru-Cu aerogel was prepared via the in situ spontaneous gelation process for hydrogel formation followed by supercritical drying. Representatively, the mixture solution of $CuCl_2$ (0.1 M) and $RuCl_3$ (0.1 M) was first injected into the deionized water (8.5 mL) under stirring for about 5 min. Subsequently, the freshly prepared $NaBH_4$ solution (0.75 M, 1.0 mL) was swiftly added into the above solution, following by stirring for 30 s. whereafter, the above system was placed in the dark for 8 h to ensure complete gelation. The obtained hydrogel was repeatedly immersed in deionized water to remove the residual impurities such as inorganic salt ions. After that, the hydrogel was exchanged with acetone, and then the Ru-Cu aerogel was obtained by CO_2 supercritical drying. Ru-Cu aerogels with different proportions were prepared by simply adjusting the proportion of the two precursor salt ions, and the molar ratios of the $RuCl_3$ and $CuCl_2$ salts were set to 5: 95, 10: 90 and 30: 70, respectively. Cu aerogel was prepared in the same way without adding Ru salt.

3. Characterization

The SEM images were provided from the FEI Nova Nano SEM 450 field emission scanning electron microscope with the accelerating voltage of 15 kV. The TEM, high resolution TEM (HRTEM), high-angle annular dark-field scanning transmission electron microscopy (HAADF-STEM) images, the selected area electron diffraction (SAED) pattern, and the energy dispersive X-ray spectrum (EDS) as well as elemental mapping images were performed on using the FEI Talos F200X transmission electron microscope under the acceleration voltage of 200 kV. The crystalline structure pattern was carried out the Shimadzu XRD-6000 powder X-ray diffractometer (XRD) with Cu Kα as the radiation source. The X-ray photoelectron spectrum (XPS) was conducted on a ThermoFisher ESCALAB 250XI to characterize the chemical compositions and the valence states. Nitrogen physisorption isotherms were tested on a Micromeritics ASAP 2460 instrument based on the Brunauer-Emmett-Teller (BET) method, and the pore size distribution was analyzed using the Barrett-Joyner-Halenda (BJH) model.

4. Electrochemical measurement

The electrocatalytic hydrogen evolution activity of Cu aerogel and Ru-Cu aerogels under acidic condition was studied in 0.5 M H_2SO_4 solution. First, the obtained aerogels were dispersed in the mixed solvents containing ethanol, deionized water, and 5 wt% Nafion solution (33: 65: 2), and vigorously sonicated for 0.5 h to form the 5 mg mL^{-1} homogeneous ink solutions. Next, the as-prepared ink was uniformly loaded onto the surface of carbon fiber paper (CFP, 0.5 × 0.5 cm^2) with the dosage of 0.2 mg, subsequently air-dried at room temperature for testing. All electrochemical experiments were carried out using CHI 660E electrochemical workstation (CHI, China) with a conventional three-electrode system in 0.5 M H_2SO_4 aqueous solution at room temperature to measure the HER performance. Among them, the as-prepared samples on CFP, a graphite plate and the Ag/AgCl (3 M KCl) were used as the working electrode, counter electrode, and reference electrode, respectively. The Ag/AgCl reference electrode was calibrated against the reversible hydrogen electrode (RHE) by the equation $E_{RHE} = E_{Ag/AgCl} + 0.215 + 0.0591 \times pH$. All linear sweep voltammetry curves were measured in 0.5 M H_2SO_4 at the scan rate of 5 mV/s and all the polarization curves were iR-corrected for all samples. The electrochemically active surface area (ECSA) of the sample was estimated from the electrochemical double layer capacitance (C_{dl}), where C_{dl} was measured by the cyclic voltammetry (CV) method under various scan rates (10, 20, 30, 40, 50, and 60 mV s^{-1}). To evaluate the electrocatalytic stability for HER, the chronoamperometry method was carried out for 18 h with different current densities. The electrochemical impedance spectrum (EIS) measurements for different samples were conducted from 100 kHz to 0.1 Hz at -0.135 V (vs RHE).

5. Theoretical calculations

The density functional theory (DFT) calculations were performed in the Vienna ab initio Simulation Package (VASP) code.[1] The electronic exchange–correlation energy is described by the spin-polarized generalized gradient approximation (GGA) with the Perdew–Burke–Ernzerhof (PBE) functional.[2, 3] The plane wave basis set was

employed with an energy cutoff at 450 eV. The vacuum of 15 Å is built between the neighboring images. A four-layer face centered cubic (4×4×4) structure of the Cu (111) was adopted in which the lattice constant was 3.61 Å. The Ru cluster of 6 atoms was placed on the Cu surface modified with oxygen atoms to simulate the surface of Ru-Cu aerogel. The convergence threshold was set as 0.02 eV per Angstrom in force. The Brillouin zone was modeled by gamma centered Monkhorst-Pack scheme, in which a 3×3×1 grid was adopted.

Each electrochemical reaction step of hydrogen evolution reaction involves a ($H^+ + e^-$) pair transfer from the adsorbed species on the surface to the electrolyte. For the calculations of $G_{H^+}+G_{e^-}$ under the normal condition (pH=0, U=0), we employ the computational hydrogen electrode (CHE) model provided by Nørskov to calculate the chemical potential of $H^+ + e^-$:

$$G_{H^+} + e^- = 1/2G_{H2}$$

The change in the Gibbs free energy of each ($H^+ + e^-$) pair transfer reaction was calculated by computational hydrogen electrode (CHE) model:

$$\Delta G = \Delta E+\Delta ZPE+\Delta H_{(0\rightarrow 298.15K)}-T\Delta S$$

In which the ΔE, Δ ZPE, $\Delta H_{(0\rightarrow 298.15K)}$ and the ΔS were referred to as the change in potential energy. Under the standard DFT calculation conditions (T = 0 K), so the T is almost negligible. Actually, when the temperatures greater than 0 K and constant pressure, that means normal temperature and pressure conditions (here T = 298.15 K). The zero-point energy was calculated by the summation of all vibrational frequencies:

$$ZPE = 1/2\sum \hbar\nu$$

where the ν corresponded to the vibrational frequency of each normal mode.

Supporting figures and tables

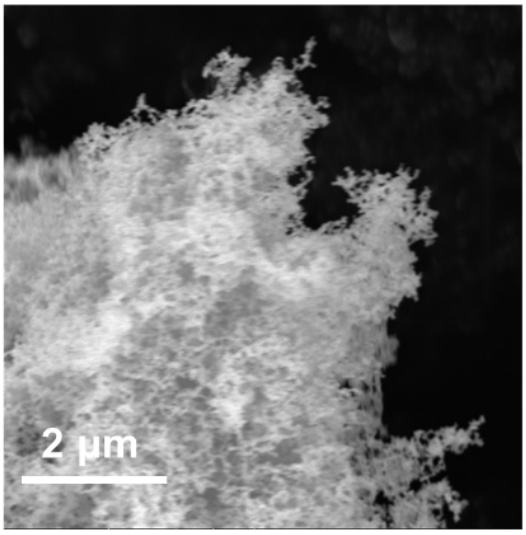

Figure S1. Representative SEM image of Cu aerogel.

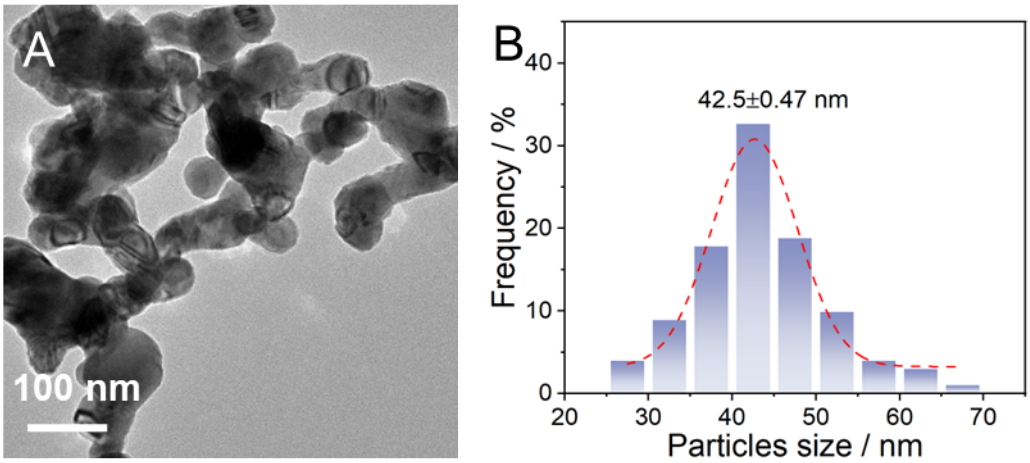

Figure S2. (a) Representative TEM image of the Cu aerogel, (b) branch size distribution.

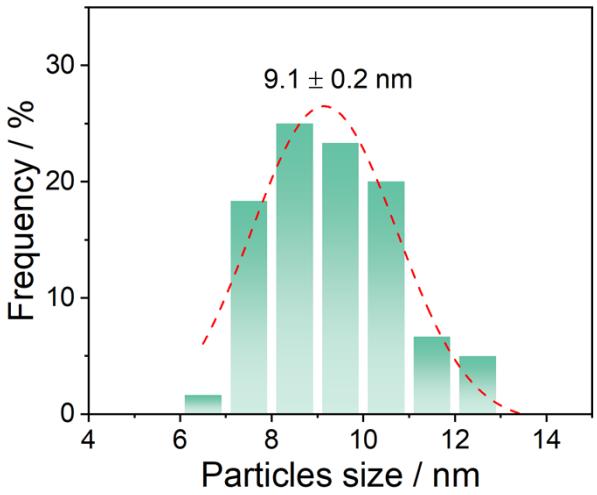

Figure S3. Size distribution of Cu nanoparticles in the Ru-Cu aerogel.

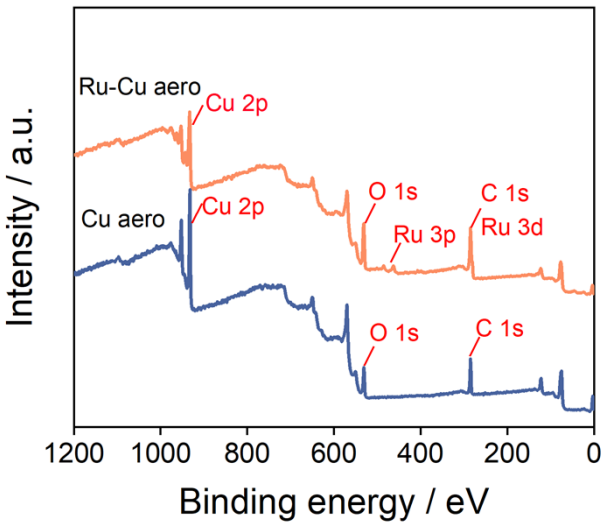

Figure S4. Wide-scan XPS spectra of the Cu and Ru-Cu aerogels.

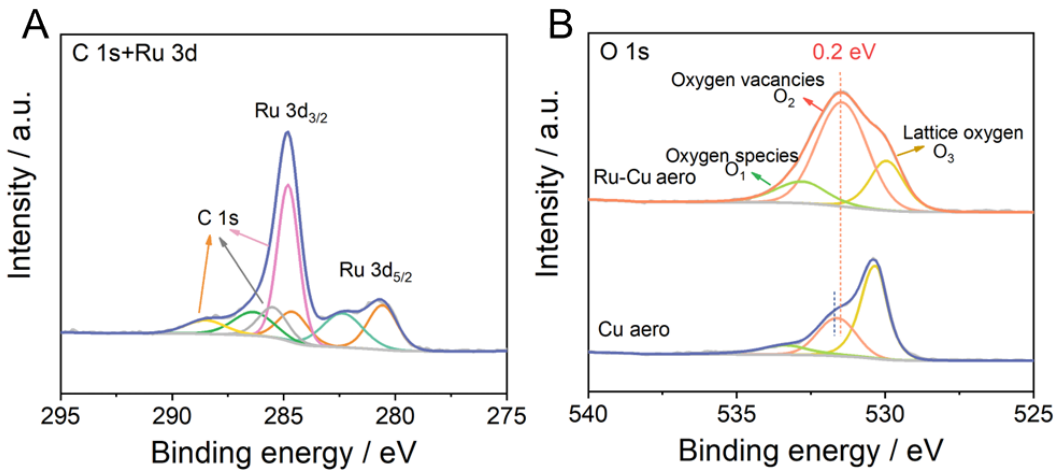

Figure S5. (a) High-resolution XPS spectra of C 1s and Ru 3d, (b) high-resolution XPS spectra of O 1s of the Cu and Ru-Cu aerogels.

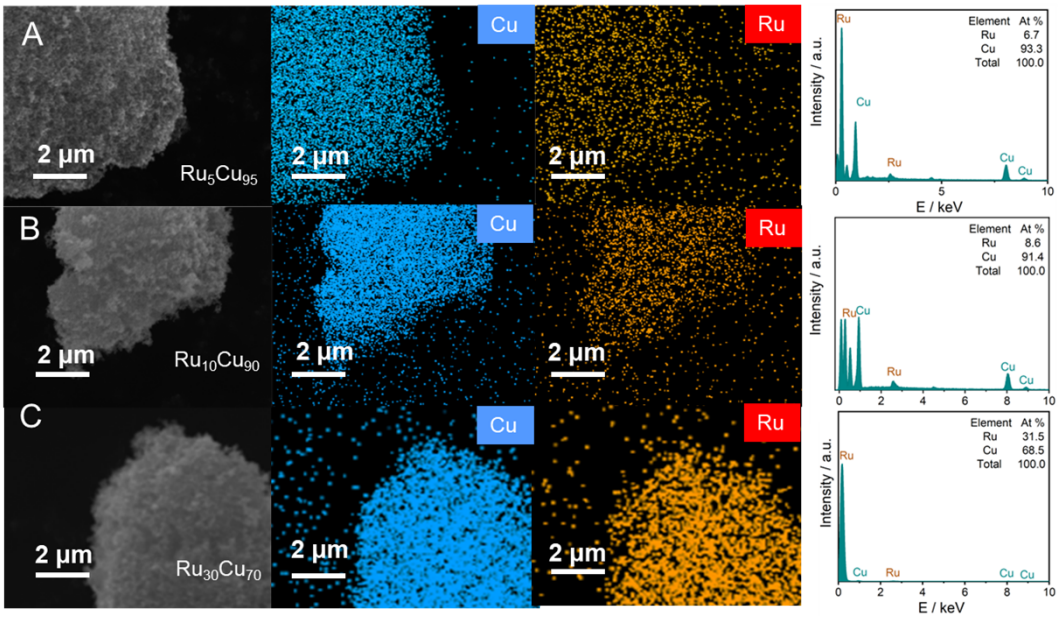

Figure S6. SEM images and corresponding elemental mappings of (a) Ru_5Cu_{95}, (b) $Ru_{10}Cu_{90}$ and (c) $Ru_{30}Cu_{70}$ aerogels.

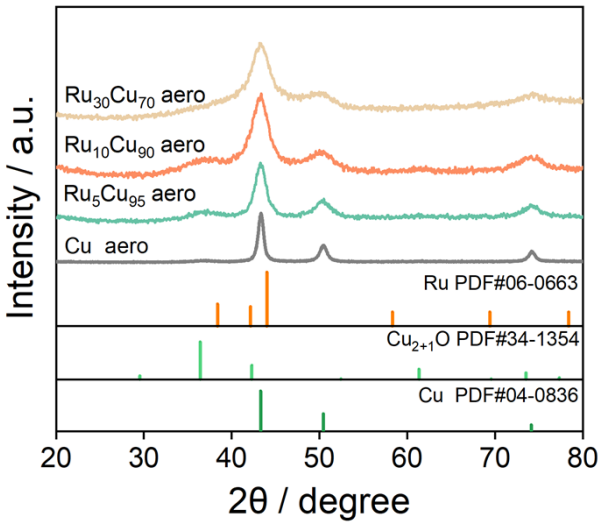

Figure S7. XRD patterns of the Cu and various Ru-Cu aerogels (Ru_5Cu_{95}, $Ru_{10}Cu_{90}$, and $Ru_{30}Cu_{70}$).

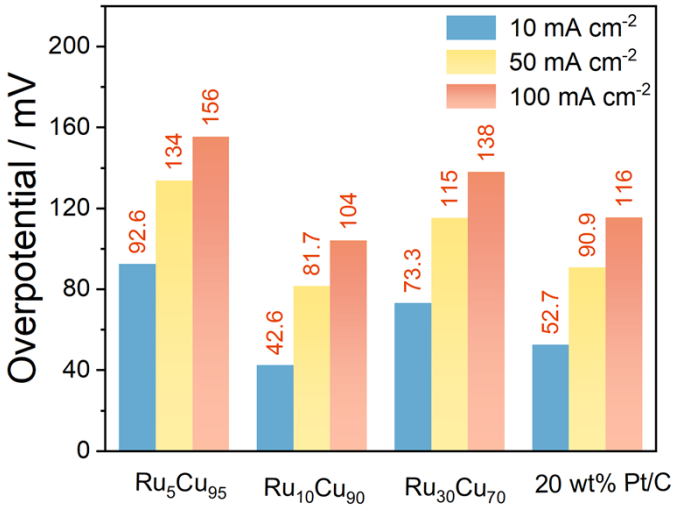

Figure S8. Comparison of overpotential observed with different catalysts at 10, 50, and 100 mA cm^{-2}.

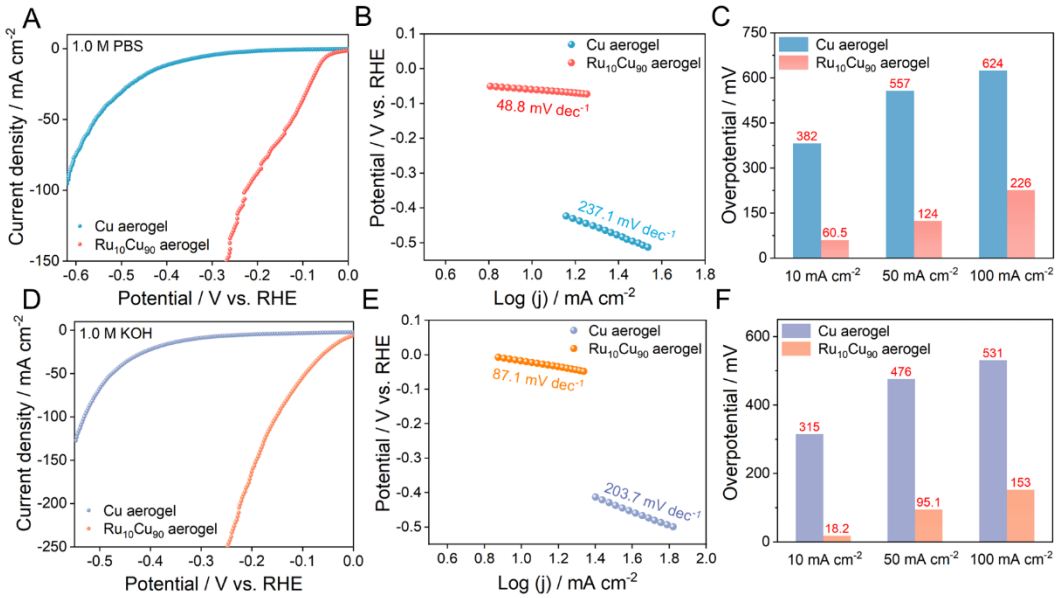

Figure S9. HER performance of Cu and $Ru_{10}Cu_{90}$ aerogel in (a, b, c) 1.0 M PBS and (d, e, f) 1.0 M KOH solutions. (a, d) Polarization curves, (b, e) corresponding Tafel plots, (c, f) and the comparison of overpotentials at 10, 50, and 100 mA cm^{-2}.

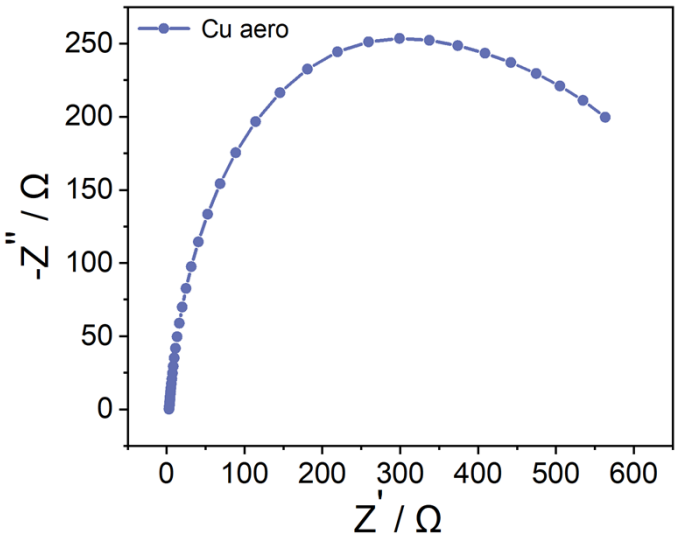

Figure S10. Nyquist plot of the Cu aerogel recorded in 0.5 M H_2SO_4 solution.

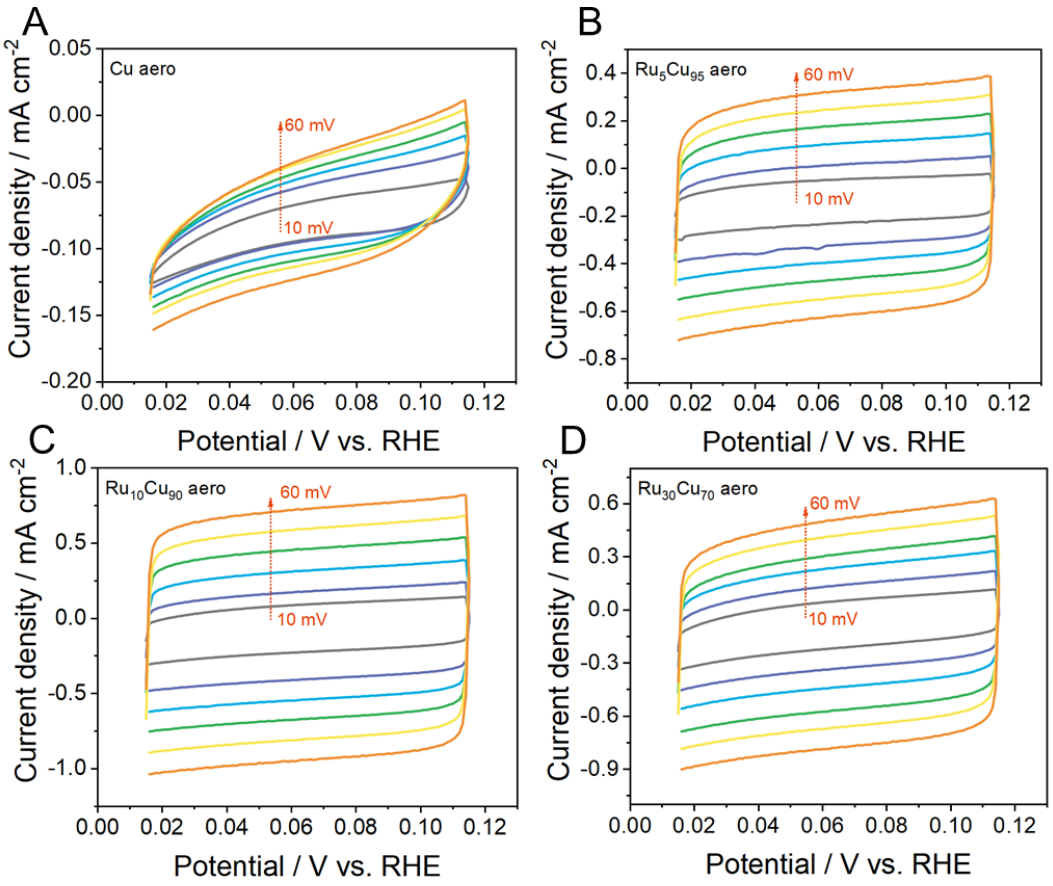

Figure S11. CV curves of Cu, Ru_5Cu_{95}, $Ru_{10}Cu_{90}$ and $Ru_{30}Cu_{70}$ aerogels in 0.5 M H_2SO_4 with different scan rates (10, 20, 30, 40, 50, and 60 mV/s), respectively.

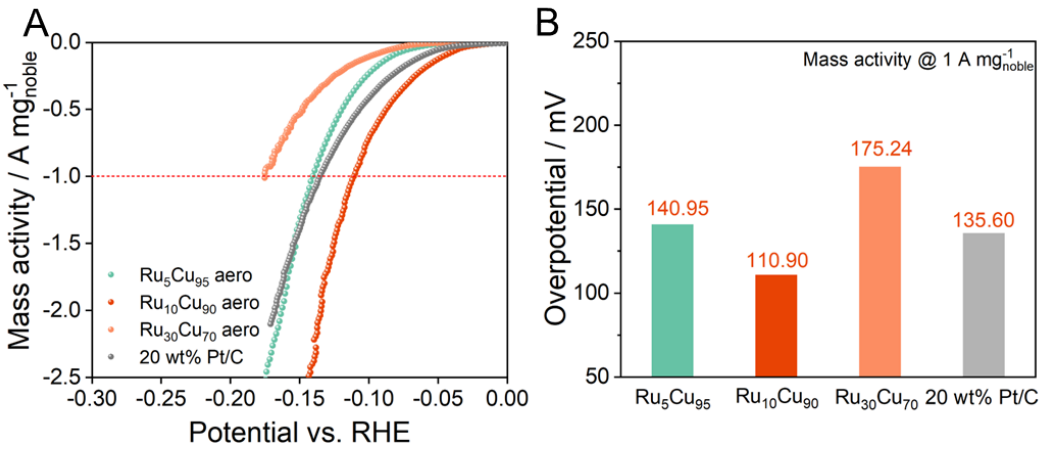

Figure S12. (a) Polarization curve after normalization to the mass activity of noble metals, (b) the mass activity at 1 A mg^{-1} of different catalysts.

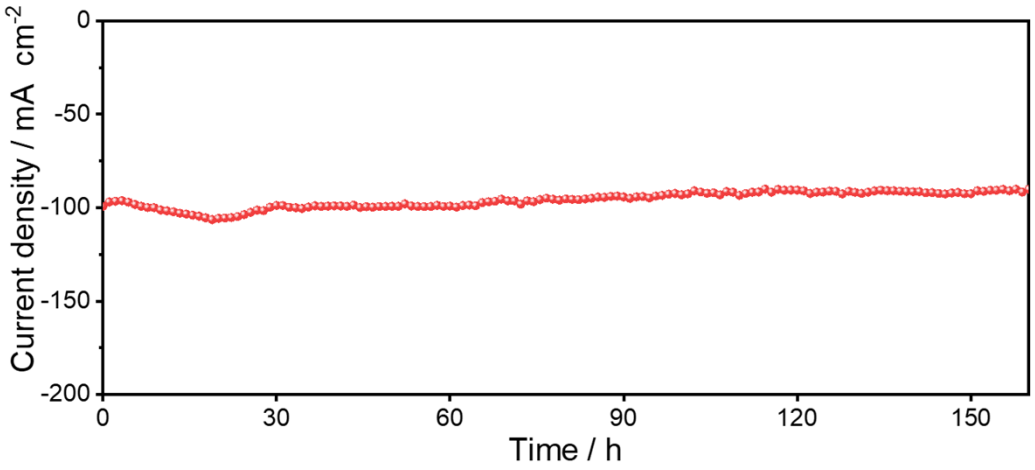

Figure S13. The i-t curve for $Ru_{10}Cu_{90}$ aerogel under the current density of 100 mA cm^{-2} for 160 h in 0.5 M H_2SO_4.

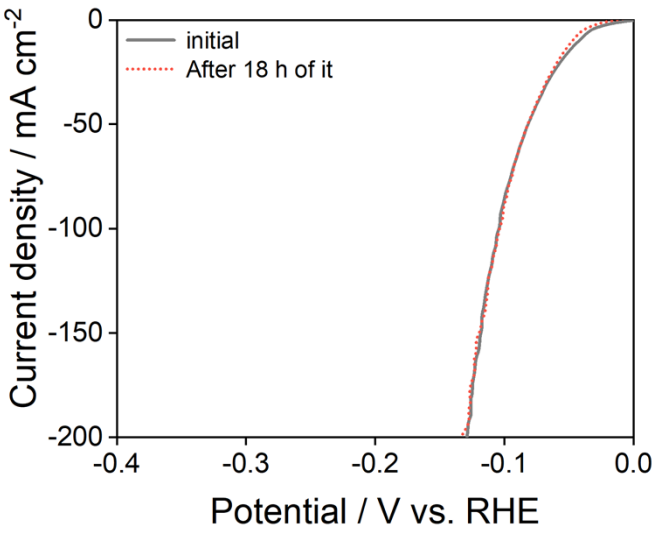

Figure S14. Polarization curve of $Ru_{10}Cu_{90}$ aerogel collected before and after long-term chronoamperometric testing under the current density of 10 mA cm^{-2}.

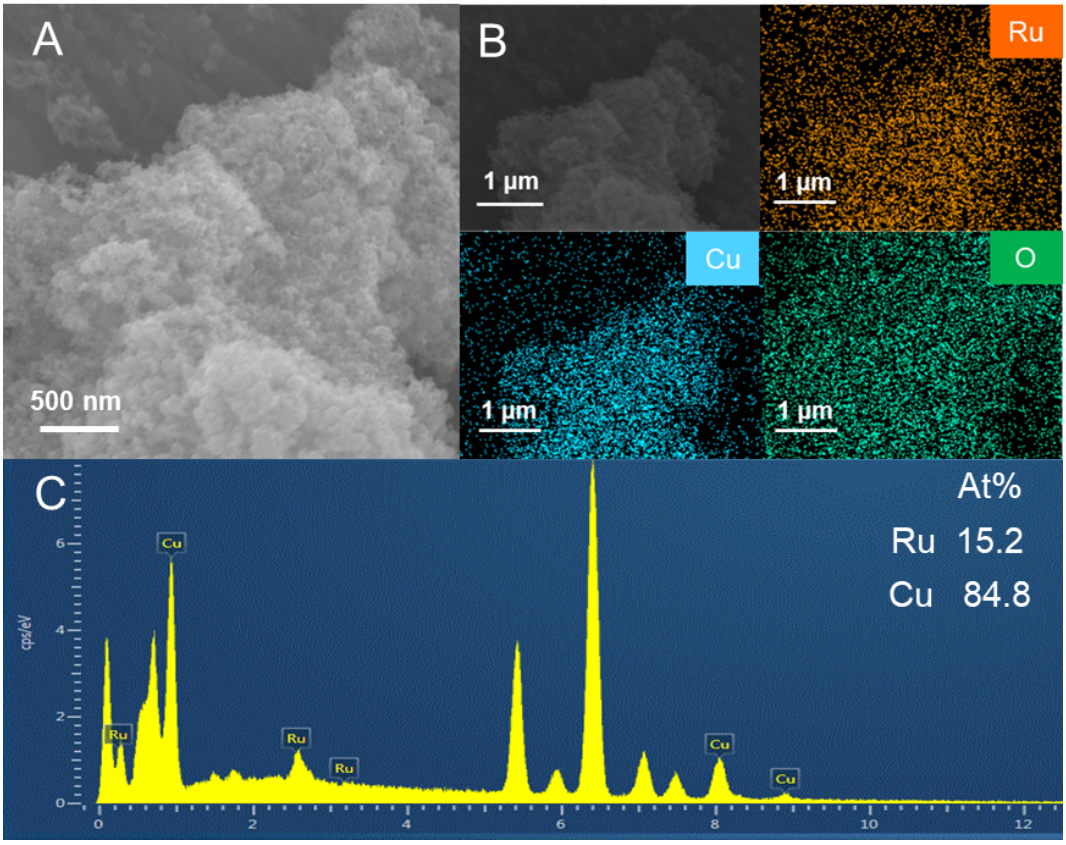

Figure S15. (a) SEM image for $Ru_{10}Cu_{90}$ aerogel collected after stability test of HER. (b) Elemental mapping images of Ru and Cu in $Ru_{10}Cu_{90}$ aerogel. (c) EDS result for $Ru_{10}Cu_{90}$ aerogel.

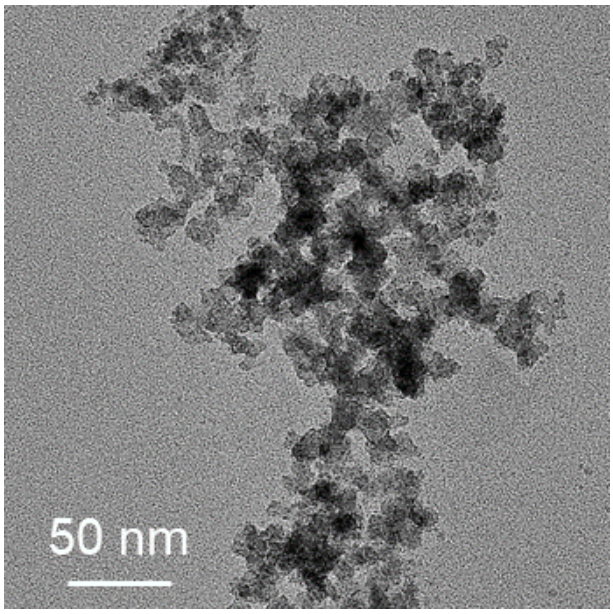

Figure S16. TEM image for $Ru_{10}Cu_{90}$ aerogel collected after stability test of HER.

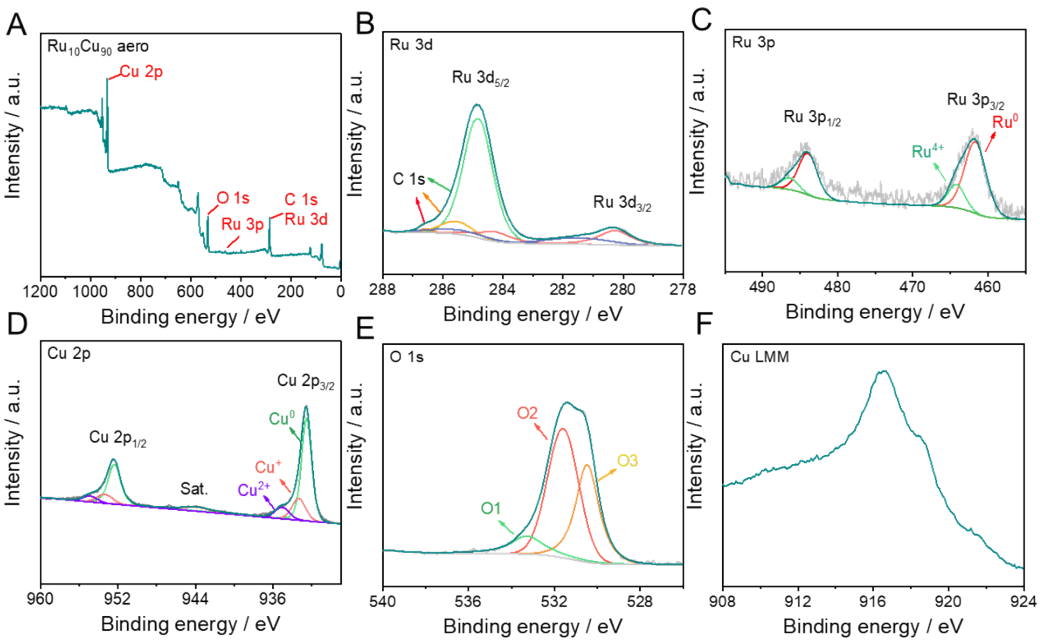

Figure S17. (a) Wide-scan XPS spectrum of $Ru_{10}Cu_{90}$ aerogel, (b-f) High-resolution XPS spectra of Ru 3d, Ru 3p, Cu 2p, O 1s and Cu LMM, respectively.

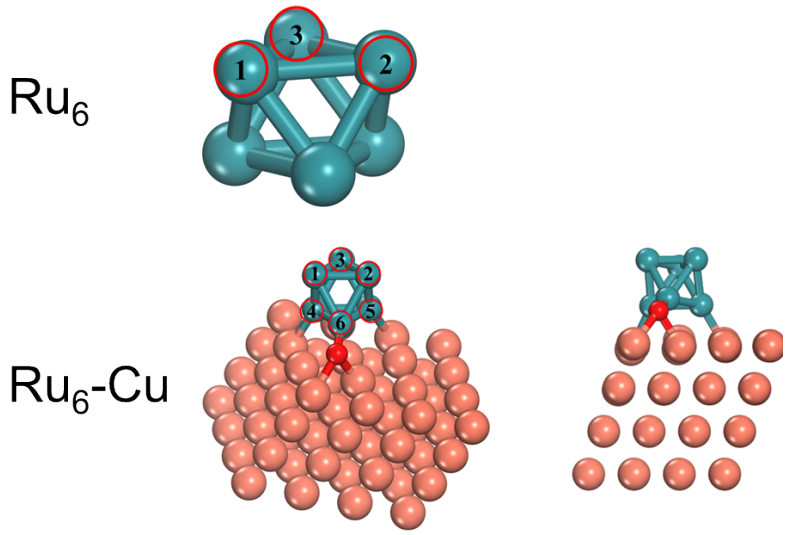

Figure S18. Structural models of the Ru-Cu aerogel and Ru cluster, Color code: Cu (orange), O (red), Ru (green).

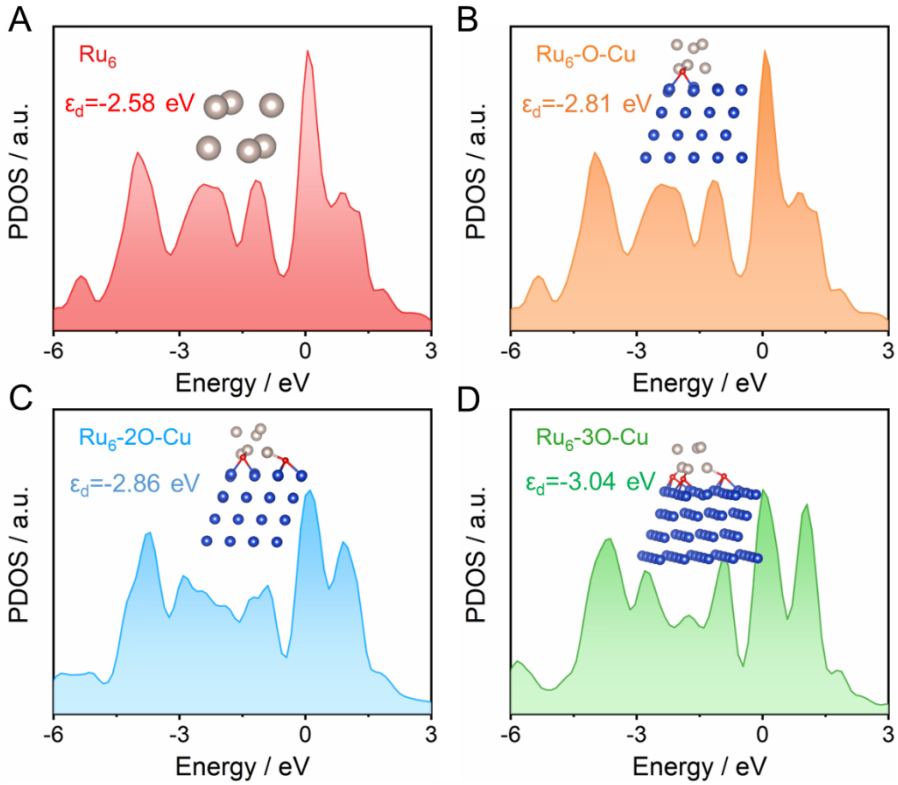

Figure S19. The PDOS of d orbitals for Ru_6 cluster, Ru_6-O-Cu, Ru_6-2O-Cu and Ru_6-3O-Cu, respectively.

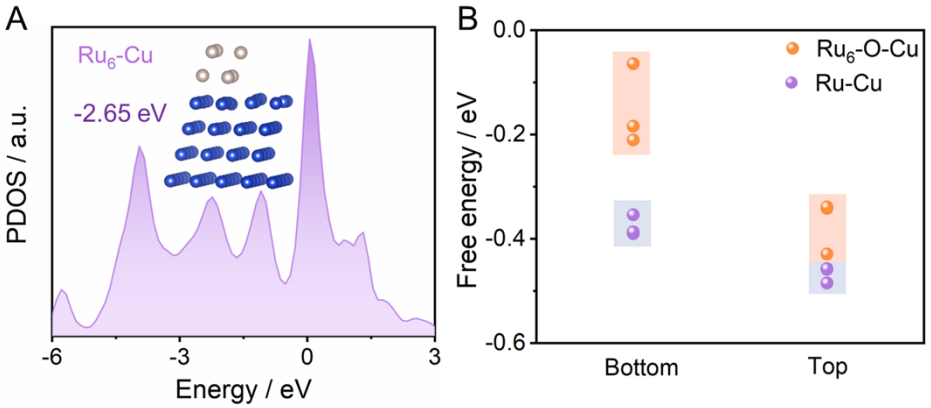

Figure S20. (a) The PDOS of d orbitals for Ru_6-Cu and (b) the Gibbs free energy for hydrogen adsorption of Ru_6-Cu and Ru_6-O-Cu at different positions.

Table S1. The percentages of O1, O2 and O3 species estimated from the O1s XPS spectra.

Catalyst	O1/(O1+O2+O3) %	O2/(O1+O2+O3) %	O3/(O1+O2+O3) %
Cu aerogel	12.50	30.68	56.82
Ru-Cu aerogel	14.56	63.29	22.15

Table S2. Fitting parameters obtained from the EIS data of different aerogels for HER at -0.135 V in 0.5 M H_2SO_4.

Catalyst	R_s (Ω)	R_{ct} (Ω)	CPE (mF)
Cu aerogel	4.34	545.8	0.365
Ru_5Cu_{95} aerogel	3.04	5.33	1.18
$Ru_{10}Cu_{90}$ aerogel	2.61	3.18	1.59
$Ru_{30}Cu_{70}$ aerogel	2.65	4.25	1.39

Table S3. Comparison of the HER performance for $Ru_{10}Cu_{90}$ aerogel with references all measured in acidic electrolyte (0.5 M H_2SO_4).

Catalyst	η /10 mA cm^{-2}	Tafel slope /mV dec^{-1}	Reference
$Ru_{10}Cu_{90}$ aerogel	42.6	38.1	This Work
Ni@Ni_2P-Ru	51	35	[12]
RuNi/CQDs	58	55	[13]
B-Ru@CNT	62	82	[14]
$RuTe_2$	35.7	46.6	[16]
Ru/HMCs-500	48.09	40.39	[17]
RuCo@HCS-500	57	48	[35]
RuB_2	52	66.9	[36]
CNT/C/Ru-700	36.2	127	[37]
Ru-RuO_2/CNT	63	31	[38]
Mo_2C-Ru/C	64	67	[39]

Table S4. The percentages of O1, O2 and O3 species for the used RuCu aerogel estimated from the O1s XPS spectrum.

Catalyst	O1/(O1+O2+O3) %	O2/(O1+O2+O3) %	O3/(O1+O2+O3) %
used-$Ru_{10}Cu_{90}$ aerogel	11.41	54.35	34.24

Table S5. Free energy at different sites of Ru_6 and Ru_6-Cu.

Theoretical model	Active site	H adsorption free energy
Ru_6-Cu	Ru_6-Cu-H_1	-0.33889565
	Ru_6-Cu-H_2	-0.34183463
	Ru_6-Cu-H_3	-0.42924829
	Ru_6-Cu-H_4	-0.06420946
	Ru_6-Cu-H_5	-0.18403938
	Ru_6-Cu-H_6	-0.23839262
Ru_6	Ru_6-H_1	-0.6215041
	Ru_6-H_2	-0.63083757
	Ru_6-H_3	-0.6314285

References:

[1] G. Kresse, J. Furthmuller, Efficiency of ab-initio total energy calculations for metals and semiconductors using a plane-wave basis set, Comp. Mater. Sci. 1996, **6**, 15-50.

[2] P. E. Blochl, Projector augmented-wave method, Phys. Rev. B. 1994, **50**, 17953.

[3] G. Kresse, D. Joubert, From ultrasoft pseudopotentials to the projector augmented-wave method, Phys. Rev. Lett Phys. Rev. B. 1999, **59**, 1758.